Photoelectron velocity-map imaging signature of structural evolution of silver-doped lead Zintl anions

Hua Xie, Zhengbo Qin, Xia Wu, Zichao Tang, and Ling Jiang

Citation: The Journal of Chemical Physics **137**, 064318 (2012); doi: 10.1063/1.4745000
View online: https://doi.org/10.1063/1.4745000
View Table of Contents: http://aip.scitation.org/toc/jcp/137/6
Published by the American Institute of Physics

Photoelectron velocity-map imaging signature of structural evolution of silver-doped lead Zintl anions

Hua Xie, Zhengbo Qin, Xia Wu, Zichao Tang,[a] and Ling Jiang[a]
State Key Laboratory of Molecular Reaction Dynamics, Dalian Institute of Chemical Physics, Chinese Academy of Sciences, 457 Zhongshan Road, Dalian 116023, China

(Received 30 May 2012; accepted 25 July 2012; published online 13 August 2012)

A set of silver-doped lead Zintl anions, $Ag@Pb_n^-$ ($n = 5$–12), have been studied using photoelectron velocity-map imaging spectroscopy and quantum chemical calculation. The structures of $Ag@Pb_n^-$ (n = 7–9, 11) built upon a square pyramid base, hitherto not considered, were assigned. Overall agreement between the experimental and calculated photoelectron spectra as well as vertical detachment energies allows for structural evolution to be established. The silver atom prefers to stay outside in the $n \leq 6$ clusters and intends to be encapsulated by the lead atoms in $n > 6$. A stable endohedral cage with bicapped square antiprism structure is formed at $n = 10$, the endohedral structure of which persists for the larger clusters. Especially, these $Ag@Pb_n^-$ anions have been found to undergo a transition between square pyramid and pentagonal pyramid molecular structures at $n = 11$. © *2012 American Institute of Physics*. [http://dx.doi.org/10.1063/1.4745000]

I. INTRODUCTION

The rich chemistry of Zintl anion (the family of multiply charged polyatomic anions formed by the heavier post-transition elements) has aroused great current interest due to its molecular beauty subsisted in shapes and its potential as building blocks for cluster-assembled thermoelectric materials.[1–4] A large number of "ligand-free" Group 14 Zintl clusters have been prepared via the synthesis in the liquid phase or the laser vaporization in the gas phase, of which geometric and electronic structures have been explored experimentally and theoretically.[5–18] In particular, the identifications of highly symmetric cage structures of the fascinating Pb_{10}^{2-}, Sn_{12}^{2-}, and Pb_{12}^{2-} clusters[10–13] intrigue and invite investigation of the metal-doped Zintl clusters[10–12,19–45] in the knowledge of whether a doped atom is endohedral or exohedral. Most of this work has involved the heavy Group 14 element species with the magic cluster size number of 10 and 12.[10–12,26–45] The $Co@Ge_{10}^{3-}$ and $Fe@Ge_{10}^{3-}$ clusters[30,31] feature an encapsulated pentagonal prismatic structure (D_{5h}), whereas the isoelectronic $Ni@Pb_{10}^{2-}$ cluster[28,29] prefers the encapsulated bicapped square antiprism structure (D_{4d}). Gas phase experiments show that the stannaspherene (Sn_{12}^{2-}) and plumbaspherene (Pb_{12}^{2-}) cages can trap the main-group and transition metals or the *f*-block elements except of potassium.[10–12] The Ba and Sr atoms are theoretically predicted to cap the Pb_{10} or Pb_{12} cage from the outside.[43]

Recent investigations have shown that, with an aid of quantum chemical calculation, photoelectron spectroscopy (PES) is very powerful in investigating the spectrum, structure, and bonding of the complex in the gas phase.[10–12,36,46] Photoelectron spectra of halogen-doped tin and lead cluster anions have been measured,[7] but no structural information is available. Several small doped Zintl anions, such as $Ag@Pb_n^-$ (n = 1–4),[23] $(Na_nSn_4)^-/(Na_nSn_4)$ (n = 0–4), and $(NaSn_m)^-/(NaSn_m)$ (m = 4–7),[24] have been primarily studied using the combined method of PES and theoretical calculation. Recent study on the $Cu@Si_n^-$ (n = 4–18) clusters[47] indicates that $Cu@Si_{12}^-$ is the smallest fully endohedral cluster, in which the copper atom is encapsulated in a distorted hexagonal prism cage, different from the $M@Sn_{12}^-$ cluster anions.[35] Here, we report a study on the structural evolution of the $Ag@Pb_n^-$ ($n = 5$–12) Zintl anions using photoelectron velocity-map imaging spectroscopy and quantum chemical calculation.

II. METHODS

A. Experimental

The experiments were carried out on the instrument including a laser ablation source, a time-of-flight mass spectrometer, and a collinear velocity-map photoelectron imaging analyzer. The details of this instrument have been described in Ref. 48 and a brief description was given below. The $Ag@Pb_n^-$ ($n = 5$–12) cluster anions were generated by laser vaporization of lead-silver alloy (Pb:Ag = 10:1 molar ratio) with high pressure helium carrier gas. The cluster anions of interest were interacted with a laser beam of 355 nm from a Nd:YAG laser for the photodetachment. The photoelectrons were recorded by a charge-coupled device camera. Each image was accumulated with 50 000–100 000 laser shots at 10 Hz repetition rate. The final raw image stood for the projection of the photoelectron density in the 3D laboratory frame onto the 2D imaging detector. The original 3D distribution was reconstructed using the Basis Set Expansion (BASEX) inverse Abel transform method, and the photoelectron spectrum was acquired by integrating the central slice of the 3D distribution.[49] The electron binding energy was calculated using $E_b = h\nu - eKE$, where $h\nu$ was the photo energy and eKE denoted the kinetic energies of the photoelectrons. The

[a]Authors to whom correspondence should be addressed. Electronic addresses: zctang@dicp.ac.cn and ljiang@dicp.ac.cn.

photoelectron imaging spectrum of Au^- at 355 nm was used to calibrate the imaging analyzer. Energy resolution of our analyzer was better than 40 meV at electron kinetic energy of 1 eV.

B. Computational

The TURBOMOLE 6.2 program[50] was used for all calculations. The BHLYP method was employed together with a triple-zeta valence basis set (def2-TZVP). Effective core potentials mdf-TZVP and mwb-TZVPext were applied to the lead and silver atoms, respectively. Initial cluster geometries were taken from the literature. If the simulated vertical detachment energies and spectra of these clusters did not match our experimental spectrum, additional geometries were created upon chemical intuition. Structure optimizations used tight convergence criteria. Structures were optimized until Cartesian gradients were smaller than 1×10^{-5} hartree/bohr and the energy change was smaller than 1×10^{-6} hartree. The self-consistent filed convergence criterion was 1×10^{-7} hartree for the energy and 1×10^{-7} a.u. for the root mean square of the density. The spin-orbit coupling effect is not included. Vibrational frequency calculations were accomplished to verify the nature of the species on the potential energy surfaces. RI-MP2/aug-cc-pVTZ-PP single point calculations on the BHLYP/TZVP structures were carried out to determine relative energies. The stick spectra of calculated vertical detachment energies were convoluted using a Gaussian line shape function with a width of 0.1 eV.

III. RESULTS AND DISCUSSION

The photoelectron velocity-map images and corresponding photoelectron spectra of $Ag@Pb_n^-$ ($n = 5$–12) at 355 nm (3.50 eV) are shown in Fig. 1. In each image, the outmost ring stands for the fastest kinetic energy of photoelectron, indicating the lowest electron binding energy in the photoelectron spectrum. The bands in each photoelectron spectrum represent the electron binding energies of photodetachment transitions from the ground state of the anionic cluster to the ground or excited states of corresponding neutral cluster. Optimized structures of $Ag@Pb_n^-$ ($n = 5$–12) are depicted in Fig. 2. Table I lists the comparison of the experimental vertical detachment energies (VDEs) of $Ag@Pb_n^-$ ($n = 5$–12) to the calculated values of three low-lying isomers. Comparison of experimental photoelectron spectrum for each individual cluster up to $n = 12$ to the simulated spectra of three low-lying isomers is given in Figs. 3–10.

As shown in Fig. 1, the photoelectron image of $Ag@Pb_5^-$ exhibits four obvious rings, resulting in four major bands in the photoelectron spectrum. In general, the spectra of $Ag@Pb_n^-$ become more compacted with the increase of cluster size. The spectra and structural assignment will be analyzed for each individual cluster based on the comparison of experimental spectrum to simulated spectra of several low-lying isomers, followed by a discussion of structural evolution.

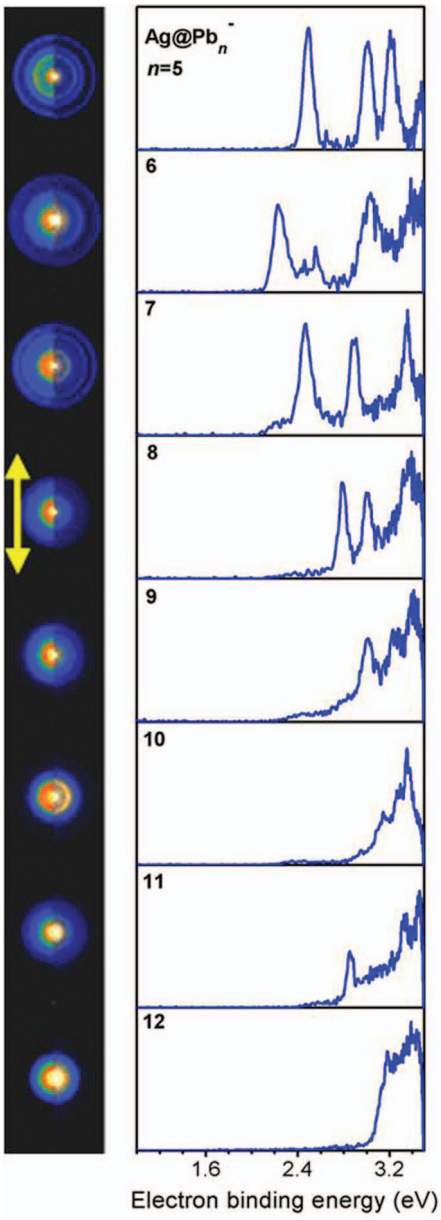

FIG. 1. Photoelectron velocity-map images (left column) and experimental photoelectron spectra (right column) of the $Ag@Pb_n^-$ ($n = 5$–12) clusters at 355 nm (3.50 eV). Each photoelectron velocity-image consists of raw image (left part) and the reconstructed image (right part) after inverse Abel transformation. The double arrow indicates the direction of the laser polarization.

A. $Ag@Pb_5^-$

In the lowest-lying structure of $Ag@Pb_5^-$ (**5A**), the silver atom is adsorbed on a bipyramid of Pb_5^- (Fig. 2), which is similar to the favorable structures of $Na@Sn_5^{0/-}$,[24] $Cu@Si_5^-$,[47] and $Ag@Si_5$.[51] The VDE of **5A** is calculated to be 2.45 eV, which is in accord with the experimental value of 2.49 eV (Table I). A planar structure (**5B**) is predicted to be 2.37 eV higher in energy than **5A**. **5C** has one silver atom adsorbed on top of a square pyramid of Pb_5, which is 3.95 eV higher in energy than **5A**. The calculated VDE values and simulated spectra of **5B** and **5C** are quite different from the experiments (Table I and Fig. 3), and these two isomers can be excluded from the assignment. It is noted that in the simulated spectrum of **5A**, two bands at 2.5 eV are too close

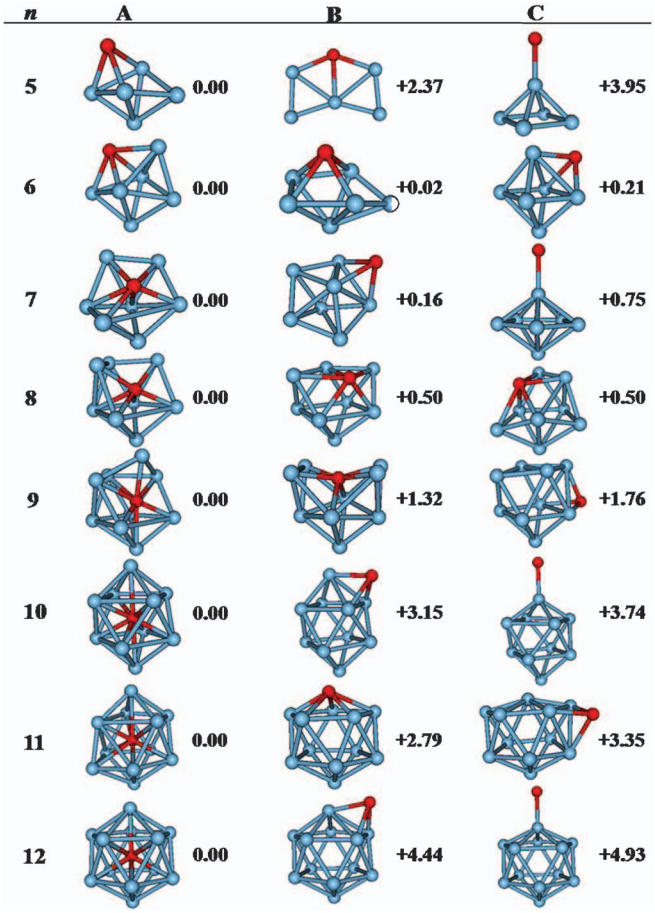

FIG. 2. Optimized structures of three low-lying isomers (***n*A**, ***n*B**, and ***n*C**) for $Ag@Pb_n^-$ ($n = 5-12$). Relative energies are given in eV. The Ag and Pb atoms are shown in red and light blue, respectively.

to be well resolved in the experiment and the intensity of band at 2.7 eV is overestimated, implying that the spin-orbit coupling shows a remarkable influence for the small lead clusters rather than for the large clusters (*vide infra*).

B. $Ag@Pb_6^-$

The calculations for $Ag@Pb_6^-$ predict three isomers (**6A**, **6B**, and **6C** in Fig. 2) of similar energy. **6A** is a pen-

TABLE I. Comparison of experimental vertical detachment energies of $Ag@Pb_n^-$ ($n = 5-12$) to the calculated values of three low-lying isomers (***n*A**, ***n*B**, and ***n*C**) shown in Fig. 2 (in eV).

		Calc.		
N	Expt.[a]	***n*A**	***n*B**	***n*C**
5	2.49(4)	2.45	2.12	1.92
6	2.23(5)	1.99	2.13	2.41
7	2.47(4)	2.52	2.06	2.47
8	2.79(3)	2.68	2.90	2.49
9	3.01(2)	2.87	2.78	2.74
10	2.95(2)	2.79	2.43	3.20
11	2.85(3)	3.07	2.84	2.59
12	3.18(1)	3.15	3.06	3.10

[a]Numbers in parentheses are experimental uncertainties in the last digit.

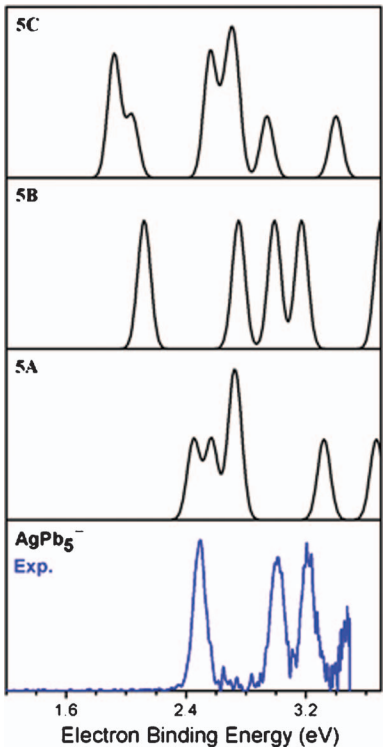

FIG. 3. Comparison of experimental photoelectron spectrum (bottom row) of $Ag@Pb_5^-$ to the simulated spectra of the isomers **5A–5C** (upper rows).

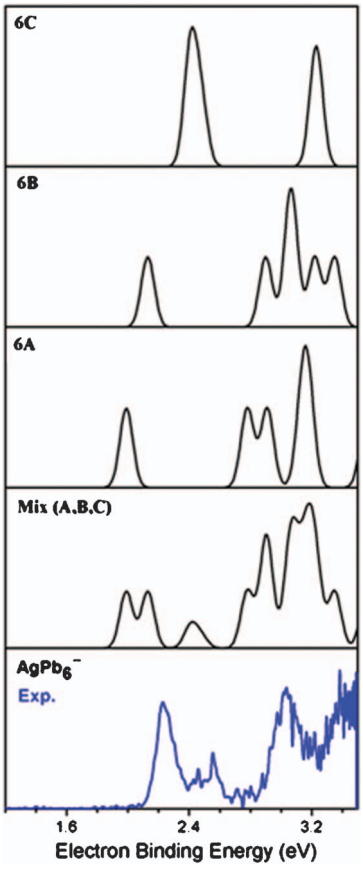

FIG. 4. Comparison of experimental photoelectron spectrum (bottom row) of $Ag@Pb_6^-$ to the simulated spectra of the isomers **6A–6C** (upper rows). The best agreement is obtained when assuming a 5:5:1 mixture of **6A**, **6B**, and **6C** (trace labeled **Mix (A, B, C)**).

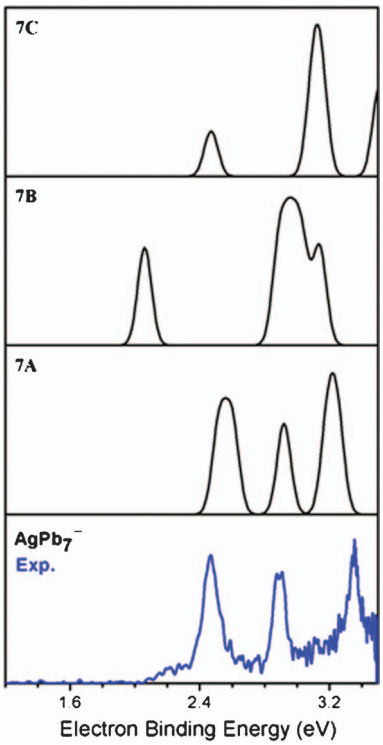

FIG. 5. Comparison of experimental photoelectron spectrum (bottom row) of $Ag@Pb_7^-$ to the simulated spectra of the isomers **7A–7C** (upper rows).

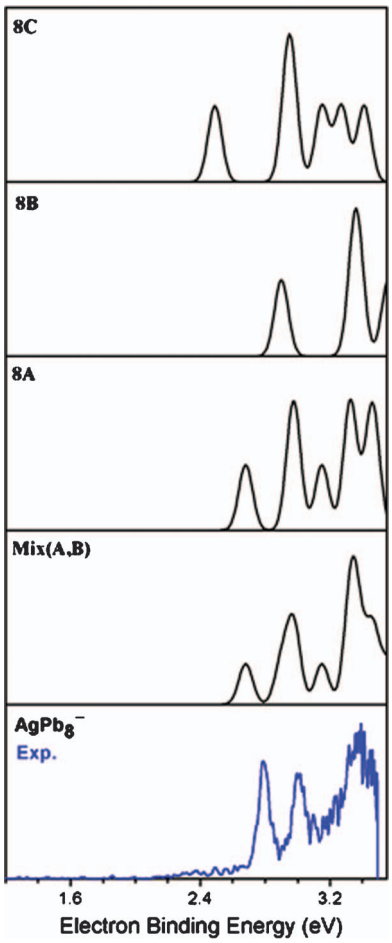

FIG. 6. Comparison of experimental photoelectron spectrum (bottom row) of $Ag@Pb_8^-$ to the simulated spectra of the isomers **8A–8C** (upper rows). The best agreement is obtained when assuming a 1:1 mixture of **8A** and 8**B** (trace labeled **Mix (A** and **B)**).

tagonal bipyramid structure in which the silver atom is a part of the pentagonal ring. The structure of **6B** could be generated by breaking one Ag–Pb bond from **6A**. In **6C**, the silver atom stays outside the Pb_6^{2-} octahedral cage. While these isomers are hard to be energetically distinguished from the BHLYP/def2-TZVP calculations (Table SI),[52] RI-MP2/aug-cc-pVTZ-PP single point calculation yields a slight preference for **6A** over **6B** by 0.02 eV and **6C** by 0.21 eV, respectively. The calculated VDE values of these three isomers are all close to the experimental data (Table I). Furthermore, the simulated spectra of **6A** and **6B** (Fig. 4) are rather similar and most of the bands have been observed in the experimental spectrum. The presence of **6C** cannot be ruled out in that the band at 2.41 eV (highest trace in Fig. 4) might account for the broad band at 2.45 eV in the experimental spectrum. A 5:5:1 mixture of **6A**, **6B**, and **6C** (trace labeled **Mix (A, B, C)** in Fig. 4) yields the best agreement. Then, the coexistence of these three isomers is likely here implying a structural change for the upcoming larger cluster.

C. $Ag@Pb_7^-$

The lowest-lying structure for $Ag@Pb_7^-$ (**7A**) is built by adding one lead atom to the edge of the most stable isomer of $Ag@Pb_6^-$ (**6A**) (Fig. 2), which has not been considered in the previous studies. **7B** is an edge-capped pentagonal bipyramid structure with the attachment of one silver atom outside, which is similar to the most stable structures of $Na@Sn_7^-$ and $Ag@Si_7$.[24,51] **7B** is only 0.16 eV higher in energy than **7A**. **7C** is a C_{5v} structure in which the silver atom sits on the top of pentagonal bipyramid, lying 0.75 eV higher in energy than **7A**. **7B** can be ruled out by the large deviation between the calculated (2.06 eV) and experimental (2.47 eV) VDE values (Table I). The band positions and overall pattern of simulated spectrum of **7A** show an obvious preference of structural assignment over **7C** (Fig. 5). Previous study shows that $Cu@Si_7^-$ prefers the **7C** structure.[47]

D. $Ag@Pb_8^-$

A new structure built by adding another lead atom onto **7A** is predicted to be the most stable isomer for $Ag@Pb_8^-$ (**8A**) (Fig. 2). The VDE of **8A** is calculated to be 2.68 eV, which is consistent with the experiment (2.79 eV) (Table I and Fig. 6). The monocapped square antiprism structure of **8B** lies only 0.50 eV higher in energy than **8A**. Another isomer (**8C**) of similar energy could be formed by a Pb_2Ag trigonal subunit glued onto the bottom of pentagonal pyramid. As compared to the experimental VDE value, the deviation for **8C** (0.3 eV) is larger than that of **8A** and **8B** (0.1 eV), respectively (Table I). Since two main bands in the simulated spectrum of **8B** are also present in the experimental spectrum, **8B** cannot be excluded. Good agreement is obtained by a 1:1 mixture of **8A** and **8B** (trace labeled **Mix(A** and **B)** in Fig. 6).

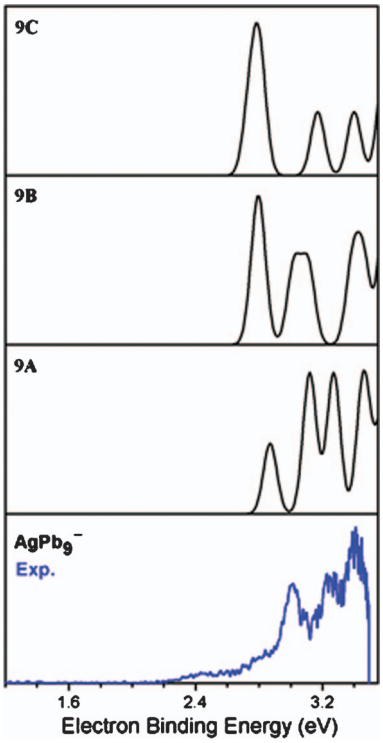

FIG. 7. Comparison of experimental photoelectron spectrum (bottom row) of $Ag@Pb_9^-$ to the simulated spectra of the isomers **9A–9C** (upper rows).

E. $Ag@Pb_9^-$

The most stable structure of $Ag@Pb_9^-$, **9A**, is built upon **8A** by filling one lead atom onto the open site or could be viewed as a precursor of the bicapped square antiprism cage by subtracting one cornered lead atom (Fig. 2). The calculated VDE value and spectrum nicely reproduce the experiments (Fig. 7). The monocapped square antiprism structure with one wrapped silver atom in one plane (**9B**) and one edge-capped silver (**9C**) lies 1.32 and 1.76 eV higher in energy above **9A**, respectively. **9B** and **9C** could be ruled out by the mismatch of the calculated VDE values and simulated spectra with the experimental ones (Table I and Fig. 7).

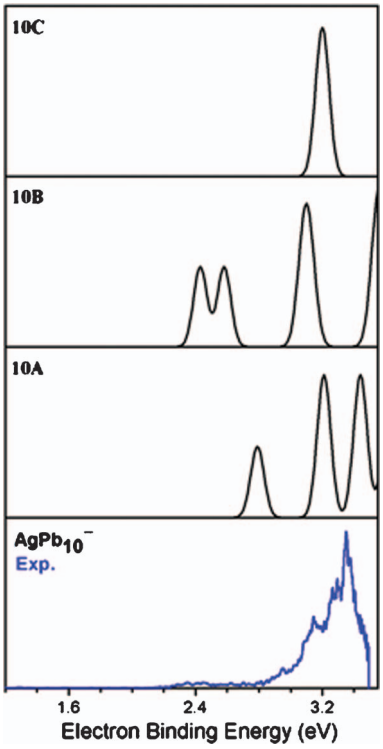

FIG. 8. Comparison of experimental photoelectron spectrum (bottom row) of $Ag@Pb_{10}^-$ to the simulated spectra of the isomers **10A–10C** (upper rows).

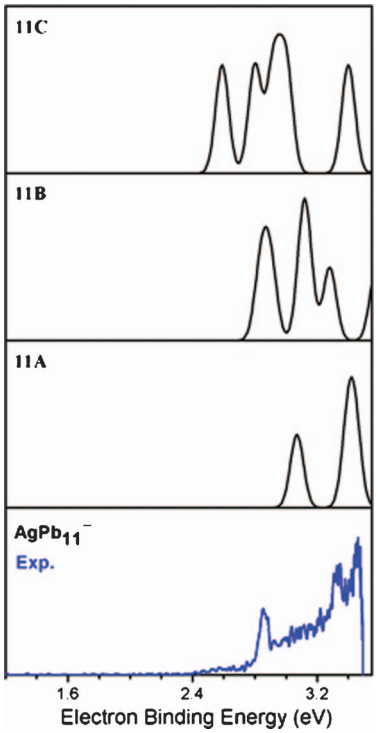

FIG. 9. Comparison of experimental photoelectron spectrum (bottom row) of $Ag@Pb_{11}^-$ to the simulated spectra of the isomers **11A–11C** (upper rows).

F. $Ag@Pb_{10}^-$

The most stable isomer of $Ag@Pb_{10}^-$, **10A**, possesses an endohedral bicapped square antiprism structure. The intensity of the band at 2.90 eV in the simulated spectrum is weakened in the experiment (Fig. 8), implying a highly stable structure. **10B** and **10C** is built upon the bicapped square antiprism structure by edge-capping and top-bonding one silver atom, respectively. The spectra of these two isomers **10B** (+3.15 eV) and **10C** (+3.74 eV) should lie too high in energy to be probed in the experiment (Table I). This suggests the overwhelming stability of **10A** as the global minimum structure of $Ag@Pb_{10}^-$, which is similar to the $Ni@Pb_{10}^{2-}$ cluster[28,29] but different from the $Co@Ge_{10}^{3-}$ and $Fe@Ge_{10}^{3-}$ clusters.[30,31]

G. $Ag@Pb_{11}^-$

The most stable isomer of $Ag@Pb_{11}^-$, **11A**, has an endohedral cage structure bearing the square and pentagonal pyramids simultaneously (Fig. 2). **11B** is a bicapped pentagonal prismatic structure in which the silver atom is a part of the cape, lying 2.79 eV higher in energy than **11A**. **11C** is a monocapped pentagonal prismatic structure in which the

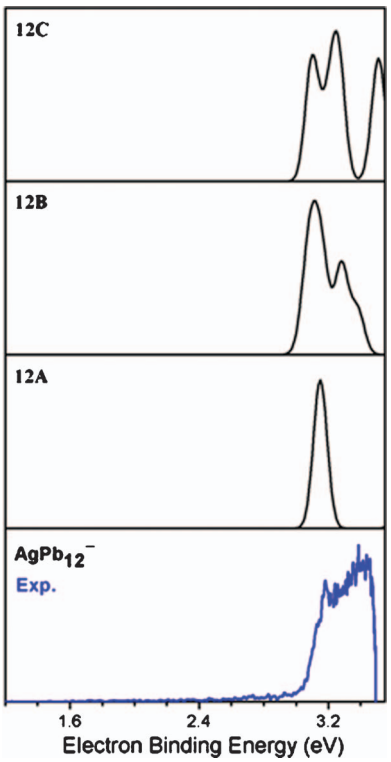

FIG. 10. Comparison of experimental photoelectron spectrum (bottom row) of $Ag@Pb_{12}^-$ to the simulated spectra of the isomers **12A–12C** (upper rows).

silver atom is edge-caped outside, which is 3.35 eV higher in energy than **11A**. The calculated VDE value and simulated spectrum of **11A** are consistent with the experiment (Table I and Fig. 9). Two energetically higher lying isomers **11B** and **11C** can be ruled out by their mismatch with the experimental spectrum.

H. $Ag@Pb_{12}^-$

The Ag-encapsulated bicapped pentagonal prismatic cage (**12A**) is predicted to be much more stable than the exohedral structures (**12B** and **12C**) (Fig. 2), which is in concert with the dominant abundance of this "magic-number" Zintl anion in the doped cluster distribution (Fig. S1).[52] Excellent agreement is obtained for the comparison of the experimental VDE value and photoelectron spectrum to the simulated ones of **12A** (Table I and Fig. 10), confirming the endohedral cage as the global minimum structure of $Ag@Pb_{12}^-$, which is similar to the $Sn_{12}^{2-}/Pb_{12}^{2-}$ cases.[10–12]

In summary, present calculations reproduce the overall patterns and main feature of the experimental spectra. For the larger clusters, a weak tail is observed at lower binding energies. Considering that the global minimum energy structures of the corresponding neutral structures are similar to their anionic clusters, the weak tail may attribute to other low-lying isomers. The preferred structures for $Ag@Pb_n^-$ (n = 5–12) are the isomers of ***n*A** (Fig. 2). It can be found that the lead atoms let the silver atom stay outside in the $n \leq 6$ clusters and intends to encapsulate the silver atom in $n > 6$, completing its encapsulation at $n = 10$ and forming a stable bicapped square antiprism cage. The endohedral structure persists for the larger clusters. Interestingly, silver-doped lead Zintl anions have been found to undergo a transition between square pyramid and pentagonal pyramid molecular structures at $n = 11$. In contrast, the endohedral structure for $Cu@Si_n^-$ is formed at $n = 12$,[47] in which the copper atom is encapsulated in a distorted hexagonal prism cage. The difference in the diameter of the cage may be responsible for such different structural pattern, and the related systematical exploration would benefit the rational design cluster-assembled materials with continuously tunable physical and/or chemical properties.

IV. CONCLUSIONS

Photoelectron velocity-map imaging spectroscopy combined with quantum chemical calculation has been employed to study the structural evolution of a set of silver-doped lead Zintl anions, $Ag@Pb_n^-$ (n = 5–12). Present DFT calculations reproduce the experimental photoelectron spectra and the overall patterns for the clusters studied here. The predicted VDE values are in 0.01–0.22 eV agreement with the experiments. The structures of $Ag@Pb_n^-$ (n = 7–9, 11) built upon a square pyramid base, hitherto not considered, were assigned. The silver atom shows the preference of staying outside in the $n \leq 6$ clusters and intends to be encapsulated by the lead atoms in $n > 6$. A stable endohedral cage with bicapped square antiprism structure is formed at $n = 10$, the endohedral structure of which persists for the larger clusters. The $Ag@Pb_n^-$ anions undergo a transition between square pyramid and pentagonal pyramid molecular structures at $n = 11$.

ACKNOWLEDGMENTS

This work was supported by the National Natural Science Foundation of China (Grant Nos. 21073186 and 21103186), the Ministry of Science and Technology of China (Grant Nos. 2011CB201301 and 2011YQ09000505), and the Chinese Academy of Sciences.

[1] E. Zintl, Angew. Chem., Int. Ed. **52**, 1 (1939).
[2] J. D. Corbett, Chem. Rev. **85**, 383 (1985).
[3] T. F. Fässler, Coord. Chem. Rev. **215**, 347 (2001).
[4] E. S. Toberer, A. F. May, and G. J. Snyder, Chem. Mater. **22**, 624 (2010).
[5] P. A. Edwards and J. D. Corbett, Inorg. Chem. **16**, 903 (1977).
[6] G. Ganteför, M. Gausa, K. H. Meiwes Broer, and H. O. Lutz, Z. Phys. D: At., Mol. Clusters **12**, 405 (1989).
[7] Y. Negishi, H. Kawamata, A. Nakajima, and K. Kaya, J. Electron. Spectrosc. Relat. Phenom. **106**, 117 (2000).
[8] C. Rajesh, C. Majumder, M. G. R. Rajan, and S. K. Kulshreshtha, Phys. Rev. B **72**, 235411 (2005).
[9] B. L. Wang, J. J. Zhao, X. S. Chen, D. N. Shi, and G. H. Wang, Phys. Rev. A **71**, 033201 (2005).
[10] L. F. Cui, X. Huang, L. M. Wang, J. Li, and L. S. Wang, J. Phys. Chem. A **110**, 10169 (2006).
[11] L. F. Cui, X. Huang, L. M. Wang, D. Y. Zubarev, A. I. Boldyrev, J. Li, and L. S. Wang, J. Am. Chem. Soc. **128**, 8390 (2006).
[12] L. F. Cui and L. S. Wang, Int. Rev. Phys. Chem. **27**, 139 (2008).
[13] A. Spiekermann, S. D. Hoffmann, and T. F. Fässler, Angew. Chem., Int. Ed. **45**, 3459 (2006).
[14] L. F. Cui, L. M. Wang, and L. S. Wang, J. Chem. Phys. **126**, 064505 (2007).
[15] C. Rajesh and C. Majumder, J. Chem. Phys. **126**, 244704 (2007).
[16] N. Shao, S. Bulusu, and X. C. Zeng, J. Chem. Phys. **128**, 154326 (2008).
[17] X. P. Li, W. C. Lu, Q. J. Zang, G. J. Chen, C. Z. Wang, and K. M. Ho, J. Phys. Chem. A **113**, 6217 (2009).

[18]R. Kelting, R. Otterstatter, P. Weis, N. Drebov, R. Ahlrichs, and M. M. Kappes, J. Chem. Phys. **134**, 024311 (2011).
[19]B. Kesanli, J. E. Halsig, P. Zavalij, J. C. Fettinger, Y. F. Lam, and B. W. Eichhorn, J. Am. Chem. Soc. **129**, 4567 (2007).
[20]Z. M. Sun, H. Xiao, J. Li, and L. S. Wang, J. Am. Chem. Soc. **129**, 9560 (2007).
[21]X. P. Xing, Z. X. Tian, H. T. Liu, and Z. C. Tang, Rapid Commun. Mass Spectrom. **17**, 1411 (2003).
[22]S. Furuse, K. Koyasu, J. Atobe, and A. Nakajima, J. Chem. Phys. **129**, 064311 (2008).
[23]X. J. Liu, B. Li, K. L. Han, S. T. Sun, X. P. Xing, and Z. C. Tang, Phys. Chem. Chem. Phys. **11**, 1043 (2009).
[24]W. J. Zheng, O. C. Thomas, J. M. Nilles, K. H. Bowen, A. C. Reber, and S. N. Khanna, J. Chem. Phys. **134**, 224307 (2011).
[25]D. L. Chen, W. Q. Tian, and C. C. Sun, Phys. Rev. A **75**, 013201 (2007).
[26]E. N. Esenturk, J. Fettinger, Y. F. Lam, and B. Eichhorn, Angew. Chem., Int. Ed. **116**, 2184 (2004).
[27]E. N. Esenturk, J. Fettinger, Y. F. Lam, and B. Eichhorn, Angew. Chem., Int. Ed. **43**, 2132 (2004).
[28]E. N. Esenturk, J. Fettinger, and B. Eichhorn, Chem. Commun. **247**, 247 (2005).
[29]E. N. Esenturk, J. Fettinger, and B. Eichhorn, J. Am. Chem. Soc. **128**, 9178 (2006).
[30]J. Q. Wang, S. Stegmaier, and T. F. Fässler, Angew. Chem., Int. Ed. **48**, 1998 (2009).
[31]B. Zhou, M. S. Denning, D. L. Kays, and J. M. Goicoechea, J. Am. Chem. Soc. **131**, 2802 (2009).
[32]S. Neukermans, E. Janssens, Z. F. Chen, R. E. Silverans, P. v. R. Schleyer, and P. Lievens, Phys. Rev. Lett. **92**, 163401 (2004).
[33]Z. F. Chen, S. Neukermans, X. Wang, E. Janssens, Z. Zhou, R. E. Silverans, R. B. King, P. v. R. Schleyer, and P. Lievens, J. Am. Chem. Soc. **128**, 12829 (2006).
[34]S. Neukermans, X. Wang, N. Veldeman, E. Janssens, R. E. Silverans, and P. Lievens, Int. J. Mass Spectrom. **252**, 145 (2006).
[35]L. F. Cui, X. Huang, L. M. Wang, J. Li, and L. S. Wang, Angew. Chem., Int. Ed. **46**, 742 (2007).
[36]A. Grubisic, H. P. Wang, X. Li, Y. J. Ko, F. S. Kocak, M. R. Pederson, K. H. Bowen, and B. W. Eichhorn, Proc. Natl. Acad. Sci. U.S.A. **108**, 14757 (2011).
[37]G. Li, X. Zhang, Z. Tang, and Z. Gao, Chem. Phys. Lett. **359**, 203 (2002).
[38]D. L. Chen, W. Q. Tian, W. C. Lu, and C. C. Sun, J. Chem. Phys. **124**, 154313 (2006).
[39]C. Rajesh and C. Majumder, Chem. Phys. Lett. **430**, 101 (2006).
[40]J. P. Dognon, C. Clavaguéra, and P. Pyykkö, Angew. Chem., Int. Ed. **46**, 1427 (2007).
[41]X. Chen, K. M. Deng, Y. Z. Liu, C. M. Tang, Y. B. Yuan, F. L. Hu, H. P. Wu, D. C. Huang, W. S. Tan, and X. Wang, Chem. Phys. Lett. **462**, 275 (2008).
[42]R. B. King, I. Silaghi-Dumitrescu, and M. M. Uţă, J. Phys. Chem. A **113**, 527 (2008).
[43]C. Rajesh and C. Majumder, J. Chem. Phys. **128**, 024308 (2008).
[44]T. B. Tai, H. M. T. Nguyen, and M. T. Nguyen, Chem. Phys. Lett. **502**, 187 (2011).
[45]T. B. Tai and M. T. Nguyen, J. Phys. Chem. A **115**, 9993 (2011).
[46]T. Waters, X.-B. Wang, and L.-S. Wang, Coord. Chem. Rev. **251**, 474 (2007).
[47]H. G. Xu, M. M. Wu, Z. G. Zhang, J. Yuan, Q. Sun, and W. Zheng, J. Chem. Phys. **136**, 104308 (2012).
[48]X. Wu, Z. B. Qin, H. Xie, R. Cong, X. H. Wu, and Z. C. Tang, Chin. J. Chem. Phys. **23**, 373 (2010).
[49]V. Dribinski, A. Ossadtchi, V. A. Mandelshtam, and H. Reisler, Rev. Sci. Instrum. **73**, 2634 (2002).
[50]TURBOMOLE v6.2 2010, a development of University of Karlsruhe and Forschungszentrum Karlsruhe GmbH, 1989-2007, TURBOMOLE GmbH, since 2007; also see http://www.turbomole.com.
[51]F. C. Chuang, Y. Y. Hsieh, C. C. Hsu, and M. A. Albao, J. Chem. Phys. **127**, 144313 (2007).
[52]See supplementary material at http://dx.doi.org/10.1063/1.4745000 for mass spectrum of the $Ag_m@Pb_n^-$ clusters and relative energies of three low-lying isomers at RI-MP2/aug-cc-pVTZ-PP and BHLYP/def2-TZVP levels.